2024 IEEE International Conference on Robotics and Automation (ICRA 2024)
May 13-17, 2024. Yokohama, Japan

Adaptive Passive Biped Dynamic Walking on Unknown Uneven Terrain

Lishen Pu, Yixuan Liu, Aiqun Zheng, Bofeng Qi and Chunquan Xu, *Member, IEEE*

***Abstract*— In this paper, we propose an adaptive controller for virtual passive biped dynamic walking on unknown uneven terrain. The adaptive controller consists of a trajectory tracking control law developed via backstepping method to mimic reference passive gait, and a slope estimator for the inclination angle of the terrain. In addition, a re-planning approach is introduced to correct the robot state off-track from the reference gait due to the terrain changes. The controller is validated through the simulations on the mixed uneven terrain consisting of varying slopes and steps. The results suggest that the controller shows comparable cost of transport and greater adaptability to terrain changes compared with certain existing methods.**

I. Introduction

Bipedal walking is a crucial mode of locomotion in the biological world. Passive biped robots have garnered considerable attention due to their superior energy performance and resemblance to human walking gaits. McGeer's concept of passive dynamic walking, introduced in 1990, showed that certain leg mechanisms can maintain stable gaits on shallow slopes without external energy input through physical models and simulations [1]. The energy lost due to friction and impact is recoverable from gravity. However, passive dynamic walking exhibits poor robustness and high sensitivity to slope variations. The limit cycle of passive dynamic walking possesses a very small basin of attraction [2]. With an increase in the slope, period-doubling and chaotic gait occur [3] [4].

Inspired by this phenomenon, researchers applied a small power source as a substitute for gravity to enable biped robots to perform more natural locomotion [5]–[7]. This results in a remarkably high energy efficiency, with a c_{mt} value (mechanical energy efficiency) close to 0.05, similar to human walking and much lower than fully-actuated bipeds. Since then, extensive research has explored passive dynamic walking, involving various foot shapes [8] [9], as well as its manifestation in robots with diverse structures like the rimless wheel [10] and the tensegrity robot [11]. Additionally, scholars have comprehensively studied the stability, limit cycles, chaos, and bifurcations of passive dynamic walking [12]–[14].

With the advancement of passive dynamic walking, active control has been employed in robots to imitate passive gaits, which is known as virtual passive dynamic walking. An effective approach is the potential energy shaping control based on the controlled symmetry [15], which allows virtual passive dynamic walking on any slope but remains a small basin of attraction. To address this defect and increase robustness, M.W.Spong et al. [16] proposed energy-based and passivity-based control (PBC). F. Asano introduced the concept of virtual gravity field and designed an energy-constraint control (ECC) method by approximating the mechanical energy differential to a constant [17] [18]. Given the property that the kinetic energy of a physical system is inversely proportional to the potential energy of the imitated passive system, a kinetic energy tracking controller (KETC) is mentioned in [19]. Y. Hu et al. [20] introduced a limit cycle tracking controller based on feedback linearization techniques so that the trajectory converged to the desired passive gait. Their research explored the essence of passive dynamic walking from different points of view. In summary, one of the effective ways to realize virtual passive dynamic walking is to design the controller by tracking the physical characteristics that can uniquely determine the passive walking gait.

There have been numerous studies on the bipedal walking on uneven terrain. Typically, the approach involving perception, motion planning, and control is mainstream [21]. Building an optimal control problem based on deviations is a common solution to this problem [22] [23]. The discussion on passive walking on uneven terrain appears to be very limited, with current controllers exhibiting very poor performance on stair. Passivity-based control [16] can exhibit robustness to slope changes by introducing the local slope determined by two-point contact. In our prior research [24], the kinetic energy tracking control can withstand a step of 5 ‰ of leg length and a slope change of 3°, but requires subsequent steps to adjust the gait. Consequently, there is a need to fill this gap.

In this paper, we present an adaptive controller design for a planar compass-like biped robot aiming to achieve stable virtual passive dynamic walking on unknown uneven terrain. To mimic the passive gait, we generate reference trajectory based on the passive dynamics of the biped robot. Specifically, we focus on the robot's ability to quickly identify the slope angle, which is critical for maintaining stable walking. Compared with existing virtual passive dynamic walking controllers, our method exhibits superior adaptability to varying slopes without premature detection, while achieving similar mechanical energy efficiency.

The rest of this paper is organized as follows. The dynamical model of a planar compass-like biped robot is

This work was supported by the National Nature Science Foundation of China under Grant No. 51775382. (*corresponding author: Chunquan Xu*)

Lishen Pu, Yixuan Liu, Bofeng Qi and Chunquan Xu are with the Department of Control Science and Engineering, Tongji University, No. 4800, Cao'an Highway, Jiading, Shanghai 201804, P. R. China (e-mail: xu@tongji.edu.cn).

Aiqun Zheng is with Shanghai New Tobacco Product Research Institute Co., Ltd, Shanghai 201315, P. R. China (e-mail: zhengaiqun@sh.tobacco.com.cn)

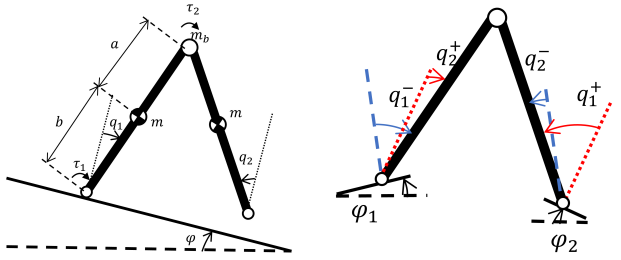

(a) (b)

Fig. 1. (a) Mathematical model of a planar compass-like biped robot. The robot's state $\boldsymbol{X}$ is defined by the two legs' angles about the slope normal $\boldsymbol{q}$ and the associated angular velocities $\dot{\boldsymbol{q}}$, $\boldsymbol{X} = [q_1, q_2, \dot{q}_1, \dot{q}_2]^T \in \mathbb{R}^4$. Default clockwise direction is positive. (b) Model of the double support phase. The slope angles before and after the impact instant are φ_1 and φ_2 respectively, resulting in a jump in the state of the biped robot from $[q_1^-, q_2^-, \dot{q}_1^-, \dot{q}_2^-]^T$ to $[q_1^+, q_2^+, \dot{q}_1^+, \dot{q}_2^+]^T$.

TABLE I
PARAMETERS OF PLANAR BIPED ROBOT

Parameter	Description	Value
a	Length of lower leg (m)	0.5
b	Length of upper leg (m)	0.5
l	Length of the whole leg (m)	1
q_1	Joint angle of the stance leg (°)	-
q_2	Joint angle of the swing leg (°)	-
m	Mass of leg (kg)	5
m_b	Mass of upper body (kg)	0
τ_1	Torque of ankle joint (Nm)	-
τ_1	Torque of hip joint (Nm)	-
J	Moment of inertia $(kg \cdot m^2)$	0.4167
φ	Slope angle (°)	-

briefly introduced in Section II. Adaptive controller design and motion planning is discussed in detail in Section III and Section IV. Simulation results and conclusion are given in Section V and Section VI, respectively.

II. MODEL AND DYNAMICS OF THE BIPEDAL WALKING

As shown in Fig. 1(a), we consider a planar compass-like biped robot driven by ankle and hip joint torques (same model as in [15]–[20]). Detailed parameter descriptions and values are provided in Table I.

During the single support phase, the motion of the robot can be described by the following nonlinear differential equation using Lagrange method:

$$\boldsymbol{M}(\boldsymbol{q})\ddot{\boldsymbol{q}} + \boldsymbol{C}(\boldsymbol{q}, \dot{\boldsymbol{q}})\dot{\boldsymbol{q}} + \boldsymbol{g}(\boldsymbol{q}, \varphi) = \boldsymbol{B}\boldsymbol{\tau} \tag{1}$$

where $\boldsymbol{q} = [q_1, q_2]^T \in \mathbb{R}^2$ is the vector of generalized coordinates composed of the joint angles, $\boldsymbol{\tau} = [\tau_1, \tau_2]^T \in \mathbb{R}^2$ is the vector of the joint torque, $\boldsymbol{M}(\boldsymbol{q}) \in \mathbb{R}^{2\times2}$ is the inertia matrix, $\boldsymbol{C}(\boldsymbol{q}, \dot{\boldsymbol{q}}) \in \mathbb{R}^{2\times2}$ is the Coriolis matrix, $\boldsymbol{g}(\boldsymbol{q}, \varphi) \in \mathbb{R}^2$ is the vector containing gravitational terms, φ represents the slope at the robot-ground contact point, $\boldsymbol{B} \in \mathbb{R}^{2\times2}$ indicates the influence of the actuators on the generalized coordinates.

Such dynamic system possesses the following property:

Property 1: The inertia matrix $\boldsymbol{M}(\boldsymbol{q})$ is symmetric and positive define matrix satisfying $\forall \boldsymbol{q} \in \mathbb{R}^2, \lambda_m \boldsymbol{I} \leq \boldsymbol{M}(\boldsymbol{q}) \leq \lambda_M \boldsymbol{I}$, where λ_m and λ_M are positive constants.

We discuss a general impact process, that is, the slopes of two adjacent steps are different, as shown in Fig. 1(b). Based on the law of conservation of angular momentum, we can derive the algebraic equations of the double support phase

$$\begin{cases} \boldsymbol{q}^+ = \Delta_{\boldsymbol{q}}\boldsymbol{q}^- - \Delta_\varphi \\ \dot{\boldsymbol{q}}^+ = \Delta_{\dot{\boldsymbol{q}}}(\boldsymbol{q}^-)\dot{\boldsymbol{q}}^- \end{cases} \tag{2}$$

where the superscript – and + denote the state before and after impacts. $\Delta_\varphi = \varphi_2 - \varphi_1$ denotes the difference between the slope of the current step and the next step. $\Delta_{\boldsymbol{q}} \in \mathbb{R}^{2\times2}$ is a constant matrix. $\Delta_{\dot{\boldsymbol{q}}}(\boldsymbol{q}^-) \in \mathbb{R}^{2\times2}$ is the impact matrix.

Combining the differential equation of the single support phase with the algebraic equation of the double support phase, we could achieve a hybrid system

$$\begin{cases} \boldsymbol{M}(\boldsymbol{q})\ddot{\boldsymbol{q}} + \boldsymbol{C}(\boldsymbol{q}, \dot{\boldsymbol{q}})\dot{\boldsymbol{q}} + \boldsymbol{g}(\boldsymbol{q}, \varphi) = \boldsymbol{B}\boldsymbol{\tau}, & (\boldsymbol{q}, \dot{\boldsymbol{q}}) \notin \mathcal{S} \\ \begin{cases} \boldsymbol{q}^+ = \Delta_{\boldsymbol{q}}\boldsymbol{q}^- - \Delta_\varphi \\ \dot{\boldsymbol{q}}^+ = \Delta_{\dot{\boldsymbol{q}}}(\boldsymbol{q}^-)\dot{\boldsymbol{q}}^- \end{cases}, & (\boldsymbol{q}, \dot{\boldsymbol{q}}) \in \mathcal{S} \end{cases} \tag{3}$$

where $\mathcal{S}$ represents a family of switch surface which is defined as

$$\mathcal{S} = \{(\boldsymbol{q}, \dot{\boldsymbol{q}}) | H(\boldsymbol{q}) = 0, \dot{H}(\boldsymbol{q}) < 0\} \tag{4}$$

where $H(\bullet)$ is defined as the height of the end of the swing leg relative to the ground. Once it is ascertained that the robot state $(\boldsymbol{q}, \dot{\boldsymbol{q}})$ falls within the predefined set $\mathcal{S}$, it can be determined that there is an impact between the swing leg and the ground.

III. ADAPTIVE CONTROLLER DESIGN

The controller framework for virtual passive dynamic walking includes a passive trajectory generator and an adaptive controller composed of a trajectory tracking controller and a slope estimator, as shown in Fig. 2.

A. Trajectory tracking control

Let the reference second-order continuous trajectory of ith step be $\boldsymbol{q}_r(t), t \in [t_i, t_i + \Delta T_i]$, where ΔT_i represents the duration of the ith step. According to the model given in Section II, the double support phase is instantaneous. Hence, only the trajectory tracking controller for the single support phase is designed.

Step 1: Consider the system (1), define the position tracking error $\boldsymbol{z}_1$ and velocity tracking error $\dot{\boldsymbol{z}}_1$ as

$$\boldsymbol{z}_1 \triangleq \boldsymbol{q}_r - \boldsymbol{q} \tag{5}$$

$$\dot{\boldsymbol{z}}_1 = \dot{\boldsymbol{q}}_r - \dot{\boldsymbol{q}} \tag{6}$$

Consider $V_1 = \frac{1}{2}\boldsymbol{z}_1^T\boldsymbol{z}_1$ as the first Lyapunov function candidate. Then, its derivative is

$$\dot{V}_1 = \boldsymbol{z}_1^T\dot{\boldsymbol{z}}_1 = \boldsymbol{z}_1^T(\dot{\boldsymbol{q}}_r - \dot{\boldsymbol{q}}) \tag{7}$$

To render (7) negative definite, $\dot{\boldsymbol{q}}$ is taken as the first virtual control. Its desired value is

$$\dot{\boldsymbol{q}}_d \triangleq \dot{\boldsymbol{q}}_r + \boldsymbol{K}_1\boldsymbol{z}_1 \tag{8}$$

where $\boldsymbol{K}_1$ is a positive definite diagonal matrix.

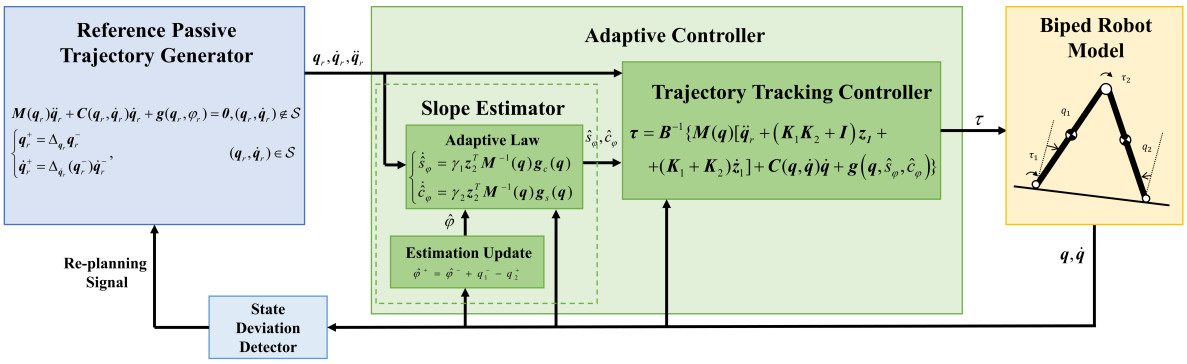

Fig. 2. Overview of the adaptive virtual passive dynamic walking controller framework. The framework contains reference passive trajectory generator (Section IV) and adaptive controller (Section III) two main components.

Step 2: The error signal involving the desired variable in (8) is defined as

$$\boldsymbol{z}_2 \triangleq \dot{\boldsymbol{q}}_d - \dot{\boldsymbol{q}} = \dot{\boldsymbol{z}}_1 + \boldsymbol{K}_1 \boldsymbol{z}_1 \tag{9}$$

The time derivative term of the error signal $\boldsymbol{z}_2$ is

$$\dot{\boldsymbol{z}}_2 = \ddot{\boldsymbol{q}}_r + \boldsymbol{K}_1(\dot{\boldsymbol{q}}_r - \dot{\boldsymbol{q}}) + \boldsymbol{M}^{-1}(\boldsymbol{q})\left[\boldsymbol{C}(\boldsymbol{q},\dot{\boldsymbol{q}})\dot{\boldsymbol{q}} + \boldsymbol{g}(\boldsymbol{q},\varphi) - \boldsymbol{B}\boldsymbol{\tau}\right] \tag{10}$$

The second Lyapunov function V_2 is considered as $V_2 = V_1 + \frac{1}{2}\boldsymbol{z}_2^T\boldsymbol{z}_2$, and its derivative is

$$\begin{aligned}\dot{V}_2 = &-\boldsymbol{z}_1^T\boldsymbol{K}_1\boldsymbol{z}_1 + \boldsymbol{z}_2^T(\boldsymbol{z}_1 + \ddot{\boldsymbol{q}}_r + \boldsymbol{K}_1\dot{\boldsymbol{z}}_1 \\ &+ \boldsymbol{M}^{-1}(\boldsymbol{q})\left[\boldsymbol{C}(\boldsymbol{q},\dot{\boldsymbol{q}})\dot{\boldsymbol{q}} + \boldsymbol{g}(\boldsymbol{q},\varphi) - \boldsymbol{B}\boldsymbol{\tau}\right])\end{aligned} \tag{11}$$

To make (11) negative definite, we chose the following control law:

$$\begin{aligned}\boldsymbol{\tau} = \boldsymbol{B}^{-1}\{&\boldsymbol{M}(\boldsymbol{q})\left[\ddot{\boldsymbol{q}}_r + (\boldsymbol{K}_1\boldsymbol{K}_2 + \boldsymbol{I})\boldsymbol{z}_1 + (\boldsymbol{K}_1 + \boldsymbol{K}_2)\dot{\boldsymbol{z}}_1\right] \\ &+ \boldsymbol{C}(\boldsymbol{q},\dot{\boldsymbol{q}})\dot{\boldsymbol{q}} + \boldsymbol{g}(\boldsymbol{q},\varphi)\}\end{aligned} \tag{12}$$

where $\boldsymbol{K}_2$ is a positive definite diagonal matrix.

B. Adaptive law for slope estimation

To facilitate the design of adaptive law to the terrain slope, we rewrite the gravity term $\boldsymbol{g}(\boldsymbol{q},\varphi)$ as follows:

$$\boldsymbol{g}(\boldsymbol{q},\varphi) = \boldsymbol{g}_c(\boldsymbol{q})s_\varphi + \boldsymbol{g}_s(\boldsymbol{q})c_\varphi \tag{13}$$

where $\boldsymbol{g}_c(\boldsymbol{q})$ and $\boldsymbol{g}_s(\boldsymbol{q})$ are related to joint angles $\boldsymbol{q}$, s_φ and c_φ stand for $\sin\varphi$ and $\cos\varphi$, respectively.

Given the slope angle is only determined by the unknown terrain in contact with the stance leg and is a constant within a step period, φ can be considered as an unknown step signal, and so be s_φ and c_φ. Let $\hat{s}_\varphi$ and $\hat{c}_\varphi$ be the estimate of s_φ and c_φ; $\tilde{s}_\varphi = s_\varphi - \hat{s}_\varphi$, $\tilde{c}_\varphi = c_\varphi - \hat{c}_\varphi$ be the estimate errors, whose derivatives satisfy $\dot{\tilde{s}}_\varphi = -\dot{\hat{s}}_\varphi$, $\dot{\tilde{c}}_\varphi = -\dot{\hat{c}}_\varphi$. Hence, according to (12), the control input τ is re-designed as follows:

$$\begin{aligned}\boldsymbol{\tau} = \boldsymbol{B}^{-1}\{&\boldsymbol{M}(\boldsymbol{q})\left[\ddot{\boldsymbol{q}}_r + (\boldsymbol{K}_1\boldsymbol{K}_2 + \boldsymbol{I})\boldsymbol{z}_1 + (\boldsymbol{K}_1 + \boldsymbol{K}_2)\dot{\boldsymbol{z}}_1\right] \\ &+ \boldsymbol{C}(\boldsymbol{q},\dot{\boldsymbol{q}})\dot{\boldsymbol{q}} + \boldsymbol{g}(\boldsymbol{q},\hat{s}_\varphi,\hat{c}_\varphi)\}\end{aligned} \tag{14}$$

To derive the optimal estimate of the slope angles which can ensure the walking stability on the unknown uneven terrain, we consider the following Lyapunov function candidate:

$$V_a = V_2 + \frac{1}{2\gamma_1}\tilde{s}_\varphi^2 + \frac{1}{2\gamma_2}\tilde{c}_\varphi^2 \tag{15}$$

where γ_1,γ_2 are positive constants. The derivative of V_a is

$$\begin{aligned}\dot{V}_a = &-\boldsymbol{z}_1^T\boldsymbol{K}_1\boldsymbol{z}_1 - \boldsymbol{z}_2^T\boldsymbol{K}_2\boldsymbol{z}_2 \\ &+ \left(\boldsymbol{z}_2^T\boldsymbol{M}^{-1}(\boldsymbol{q})\boldsymbol{g}_c(\boldsymbol{q}) - \frac{1}{\gamma_1}\dot{\hat{s}}_\varphi\right)\tilde{s}_\varphi \\ &+ \left(\boldsymbol{z}_2^T\boldsymbol{M}^{-1}(\boldsymbol{q})\boldsymbol{g}_s(\boldsymbol{q}) - \frac{1}{\gamma_1}\dot{\hat{c}}_\varphi\right)\tilde{c}_\varphi\end{aligned} \tag{16}$$

Since the first two items are negative definite, we restrict the last two items to zero by selecting the following adaptive laws for adjusting $\dot{\hat{s}}_\varphi$ and $\dot{\hat{c}}_\varphi$:

$$\begin{cases}\dot{\hat{s}}_\varphi = \gamma_1\boldsymbol{z}_2^T\boldsymbol{M}^{-1}(\boldsymbol{q})\boldsymbol{g}_c(\boldsymbol{q}) \\ \dot{\hat{c}}_\varphi = \gamma_2\boldsymbol{z}_2^T\boldsymbol{M}^{-1}(\boldsymbol{q})\boldsymbol{g}_s(\boldsymbol{q})\end{cases} \tag{17}$$

C. Stability analysis

In this part, we analyze the trajectory tracking stability and slope estimation convergence of the controller (14) with the adaptive law (17) considering the hybrid system (3).

First, define the following error variables:

$$\boldsymbol{x} = \begin{bmatrix}\boldsymbol{z}_1 \\ \boldsymbol{z}_2\end{bmatrix}, \tilde{\boldsymbol{\theta}} = \begin{bmatrix}\tilde{s}_\varphi \\ \tilde{c}_\varphi\end{bmatrix}, \boldsymbol{\eta} = \begin{bmatrix}\boldsymbol{x} \\ \tilde{\boldsymbol{\theta}}\end{bmatrix}$$

where $\boldsymbol{x}$, $\tilde{\boldsymbol{\theta}}$ represent the system state error and the estimate error of the slope angle, respectively. $\boldsymbol{\eta}$ is the augmented state variable of the system.

Double Support phase. Firstly, we analyze the evolution of $\boldsymbol{\eta}$ at the moment of impact. Because only the joint velocity jumps at this moment, we concentrate on the evolution of $\boldsymbol{x}$

$$\begin{aligned}\|\boldsymbol{x}_i^+\|^2 &= \|\boldsymbol{z}_{1,i}^+\|^2 + \|\boldsymbol{z}_{2,i}^+\|^2 \\ &= \|\boldsymbol{z}_{1,i}^+\|^2 + \|\dot{\boldsymbol{z}}_{1,i}^+ + \boldsymbol{K}_{1,i}\boldsymbol{z}_{1,i}^+\|^2 \\ &\le \left(2\lambda_{1,i}^2 + 1\right)\|\boldsymbol{z}_{1,i}^+\|^2 + 2\|\dot{\boldsymbol{z}}_{1,i}^+\|^2\end{aligned} \tag{18}$$

where $\lambda_{1,i}$ stands for the maximum eigenvalue of $\boldsymbol{K}_{1,i}$. The subscript i represents the ordinal number of the steps and the superscript – and + denote the state before and after impact. According to [20], we have the following conclusion:

$$\|\dot{\boldsymbol{z}}_{1,i}^+\| \le \alpha_i\|\boldsymbol{z}_{1,i}^-\| + \beta_i\|\dot{\boldsymbol{z}}_{1,i}^-\| \tag{19}$$

where α_i, β_i are only determined by the reference trajectory and the actual state at the moment of impact.

Thus, $\boldsymbol{x}_i^+$ and $\boldsymbol{x}_i^-$ have the following relationship:

$$\begin{aligned}\|\boldsymbol{x}_i^+\|^2 \leq & \left(2\lambda_{1,i}^2+1\right)\|\boldsymbol{z}_{1,i}^-\|^2+2\left(\alpha_i\|\boldsymbol{z}_{1,i}^-\|+\beta_i\|\dot{\boldsymbol{z}}_{1,i}^-\|\right)^2 \\ \leq & \left(2\lambda_{1,i}^2+4\alpha_i^2+1\right)\|\boldsymbol{z}_{1,i}^-\|^2+4\beta_i^2\|\dot{\boldsymbol{z}}_{1,i}^-\|^2 \\ \leq & \left(2\lambda_{1,i}^2+8\beta_i^2\lambda_{1,i-1}^2+4\alpha_i^2+1\right)\|\boldsymbol{z}_{1,i}^-\|^2+8\beta_i^2\|\boldsymbol{z}_{2,i}^-\|^2 \\ \leq & k_{\Delta,i}^2\|\boldsymbol{x}_i^-\|^2\end{aligned} \tag{20}$$

where $k_{\Delta,i}^2=\max\left(2\lambda_{1,i}^2+8\beta_i^2\lambda_{1,i-1}^2+4\alpha_i^2+1,8\beta_i^2\right)>1$. In addition, double support phase is instantaneous and will not cause a jump in slope estimate error, which suggests that

$$\|\boldsymbol{\eta}_i^+\| \leq k_{\Delta,i}\|\boldsymbol{\eta}_i^-\| \tag{21}$$

Single support phase. Next, we analyze the evolution of $\boldsymbol{\eta}$ during the single support phase. Referring to (9), (10), (14), and (17), we can obtain a linear time-varying system presented as follows:

$$\begin{bmatrix}\dot{\boldsymbol{x}}\\ \dot{\tilde{\boldsymbol{\theta}}}\end{bmatrix}=\begin{bmatrix}\boldsymbol{K} & \boldsymbol{W}^T(t)\\ -\boldsymbol{\Gamma}\boldsymbol{W}(t) & \boldsymbol{O}\end{bmatrix}\begin{bmatrix}\boldsymbol{x}\\ \tilde{\boldsymbol{\theta}}\end{bmatrix} \tag{22}$$

where

$$\boldsymbol{K}=\begin{bmatrix}-\boldsymbol{K}_1 & \boldsymbol{I}\\ -\boldsymbol{I} & -\boldsymbol{K}_2\end{bmatrix},\boldsymbol{\Gamma}=\begin{bmatrix}\gamma_1 & 0\\ 0 & \gamma_2\end{bmatrix}$$

$$\boldsymbol{W}(t)=\begin{bmatrix}\boldsymbol{O}_{2\times 2} & \begin{bmatrix}\boldsymbol{g}_c^T(\boldsymbol{q}(t))\\ \boldsymbol{g}_s^T(\boldsymbol{q}(t))\end{bmatrix}\boldsymbol{M}^{-1}(\boldsymbol{q}(t))\end{bmatrix}$$

According to Property 1, the inverse inertia matrix $\boldsymbol{M}^{-1}(\boldsymbol{q}(t))$ is both positive definite and bounded. By definition, $\boldsymbol{g}(\boldsymbol{q},\varphi)$ is bounded, and so are $\boldsymbol{g}_c^T(\boldsymbol{q}(t))$ and $\boldsymbol{g}_s^T(\boldsymbol{q}(t))$. Consequently, all terms in the excitation signal $\boldsymbol{W}(t)$ are bounded. It follows from (13) that the vector group of $\boldsymbol{W}(t)$ remains linearly independent except for specific singular points. Thus, for all $t>0$ there are positive constants λ_{α_1}, λ_{α_2} and δ such that $\lambda_{\alpha_2}\boldsymbol{I}\leq\int_t^{t+\delta}\boldsymbol{W}(s)\boldsymbol{W}^T(s)ds\leq\lambda_{\alpha_1}\boldsymbol{I}$, which indicates that the signal $\boldsymbol{W}(t)$ satisfies the persistent excitation (PE) condition. Based on the previously mentioned controller design, $\boldsymbol{K}$ is Hurwitz. Moreover, the initial state of η is bounded. Based on the findings in [25], we can further infer that the evolution of $\|\boldsymbol{\eta}\|$ in the ith step is exponentially stable

$$\|\boldsymbol{\eta}(t)\|\leq k_{C,i}e^{-\lambda_{\alpha,i}(t-t_i)}\|\boldsymbol{\eta}_i^+\|,t\in(t_i,t_i+\Delta T_i) \tag{23}$$

for positive constants $k_{C,i}$ and $\lambda_{\alpha,i}$.

Theorem 1: For a biped robot system (3) walking on an unknown slope, under the control of the trajectory tracking controller (14) with the adaptive law (17), if the parameters $\boldsymbol{K}_{1,i},\boldsymbol{K}_{2,i}$ of the ith step satisfies the following condition:

$$k_{\Delta,i}k_{C,i}e^{-\lambda_{\alpha,i}\Delta T_i}<1 \tag{24}$$

then the robot asymptotically tracks the reference trajectory, and the estimate error converges to zero.

Proof: Combining (21) and (23), we can derive the following inequation:

$$\|\boldsymbol{\eta}_{i+1}^-\|\leq k_{\Delta,i}k_{C,i}e^{-\lambda_{\alpha,i}\Delta T_i}\|\boldsymbol{\eta}_i^-\| \tag{25}$$

where $k_{C,i}$ and $\lambda_{\alpha,i}$ are positive constants. Then according to (24), we have

$$\|\boldsymbol{\eta}_{i+1}^-\|<\|\boldsymbol{\eta}_i^-\| \tag{26}$$

Referring to the multiple Lyapunov function method [26], it can be deduced that the norm of the error vector $\boldsymbol{\eta}$ is bounded and it approaches zero as $t\to\infty$, which indicates that the biped robot is capable of achieving stable locomotion. Additionally, the adaptive law accurately estimates the actual incline of the terrain. ■

D. Estimation update strategy

After each double support phase, according to (2), if $\left|q_1^--q_2^+\right|>\epsilon$ is satisfied, where ϵ is a small threshold, it is regarded that the slopes of the two adjacent steps are different. Subsequently, the slope angle estimate, denoteded as $\hat{\varphi}=\arcsin\hat{s}_\varphi$, can take the following update strategy:

$$\hat{\varphi}^+=\hat{\varphi}^-+q_1^--q_2^+ \tag{27}$$

where $\hat{\varphi}^-$ and $\hat{\varphi}^+$ are the slope estimates representing the end of the previous step and the beginning of the current step.

IV. Motion Planning Based on Passive Dynamics

A. Reference passive trajectory generation

To make the robot imitate the passive dynamic walking, the reference trajectory $\boldsymbol{q}_r(t)$ of the proposed controller (14) should be a limit cycle solution of the passive dynamical model as follows:

$$\begin{cases}\boldsymbol{M}(\boldsymbol{q}_r)\ddot{\boldsymbol{q}}_r+\boldsymbol{C}(\boldsymbol{q}_r,\dot{\boldsymbol{q}}_r)\dot{\boldsymbol{q}}_r+\boldsymbol{g}(\boldsymbol{q}_r,\varphi_r)=\boldsymbol{0}, & (\boldsymbol{q}_r,\dot{\boldsymbol{q}}_r)\notin\mathcal{S}\\ \begin{cases}\boldsymbol{q}_r^+=\Delta_{\boldsymbol{q}_r}\boldsymbol{q}_r^-\\ \dot{\boldsymbol{q}}_r^+=\Delta_{\dot{\boldsymbol{q}}_r}(\boldsymbol{q}_r^-)\dot{\boldsymbol{q}}_r^-\end{cases}, & (\boldsymbol{q}_r,\dot{\boldsymbol{q}}_r)\in\mathcal{S}\end{cases} \tag{28}$$

This formula expresses the passive dynamic walking of an unpowered biped robot on a gentle slope φ_r. According to our previous work [27], when φ_r is in the range of (0°,2.72°), the biped robot can exhibit a single-period stable motion.

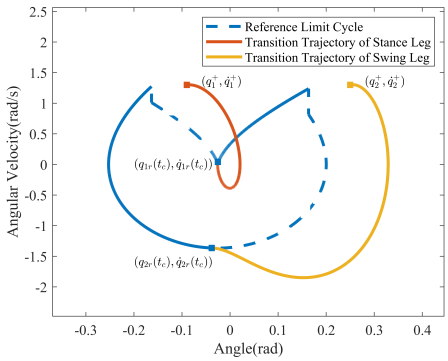

Fig. 3. The schematic diagram of the re-planning. Red and yellow solid curves are the transition trajectories of the stance leg and the swing leg respectively, which are obtained by connecting the off-track state with the reference limit cycle by Bézier curve.

B. Re-planning strategy

According to (9)(17), the adaptive law is closely associated with z_2, which depends on the velocity and position tracking errors. To minimize the impact of large z_2 caused by terrain change, a re-planning method is designed to connect the off-track state with the expected limit cycle, as demonstrated in Fig. 3. The blue curve (including both the blue solid line and the blue dotted line) represents the limit cycle of the reference trajectory (it should be noted that the phase trajectories of the swing leg and the stance leg together form the reference limit cycle). The two points $(q_1^+, \dot{q}_1^+)$ and $(q_2^+, \dot{q}_2^+)$ denote the robot's state after the impact. A delay time $t_c = \zeta \Delta T, \zeta \in (0, 1]$ is selected at first, which corresponds to two points $(q_{1r}(t_c), \dot{q}_{1r}(t_c))$ and $(q_{2r}(t_c), \dot{q}_{2r}(t_c))$ on the reference limit cycle. Then, two Bézier curves connecting the current off-track state to the two points on the reference limit cycle are constructed. The red and yellow solid curves denote the re-planned transition trajectories for the stance leg and the swing leg, respectively.

V. Simulation Results and Discussions

A. Comparison with energy-based methods

We compare our proposed controller with energy-based virtual passive dynamic walking controllers: PBC [16], ECC [17], and KETC [19]. Simulations cover five terrains: level ground, two stair grounds with tread depths of 1.8m and fixed step heights of 0.006m (stair 1) and 0.06m (stair 2), and two slope grounds with fixed slope lengths of 1.5m and continuous slope angles changing by 0.3° (slope 1) and -1° (slope 2). The biped robot mimics reference passive dynamic walking on a 2° slope throughout all simulations. Comparison results are detailed in Table II. "✗" denotes instability during walking.

The theoretical value of c_{mt} for passive dynamic walking on a slope with angle φ_r is $\sin \varphi_r$, which equals 0.0349 in this case. The c_{mt} of our proposed method is closer to the reference value on the level ground, the same as KETC. This may be attributed to the fact that the trajectory tracking and kinetic energy tracking mimics the characteristics of passive gaits more accurately than mechanical energy tracking. All methods demonstrate similar energy efficiency on uneven terrains. However, on more challenging terrains (stair 2 and slope 2), the trajectory-based method proposed in this paper exhibits superior adaptability.

TABLE II
Comparison on c_{mt}

Methods	Energy-based			Trajectory-based
	PBC	ECC	KETC	Proposed
Level	0.0342	0.0352	0.0350	0.0350
Stair 1	0.0362	0.0361	0.0363	0.0357
Stair 2	✗	✗	✗	0.0831
Slope 1	0.0336	0.0338	0.0339	0.0336
Slope 2	✗	0.0353	✗	0.0335

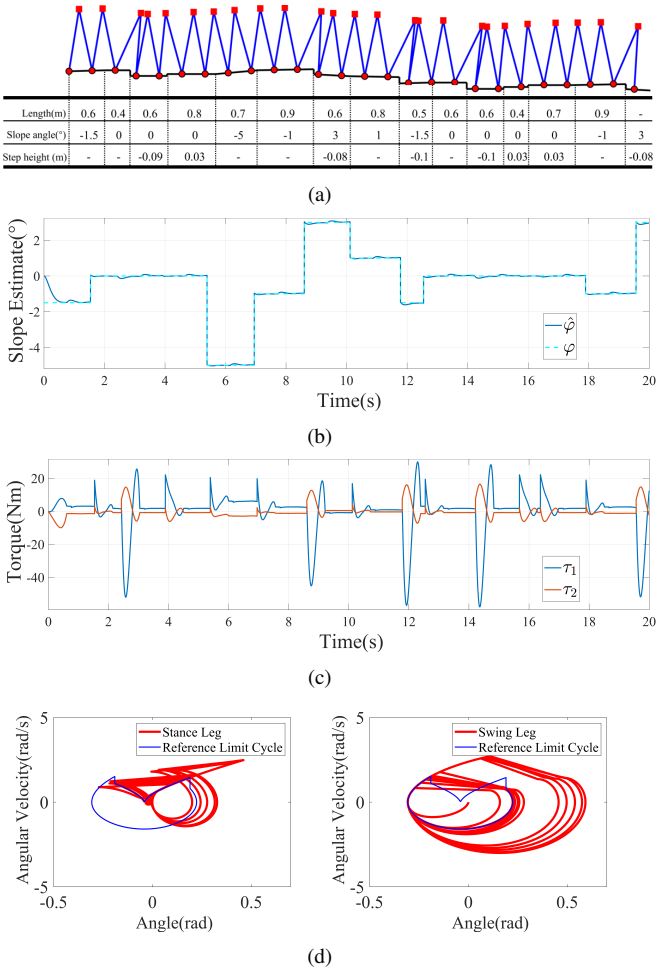

Fig. 4. Simulation results of the virtual passive dynamic walking on a mixed terrain with various slopes and steps. (a) Time lapse animation of each step, with the terrain parameters listed below. The downward slope angle and the upward step height are positive. The step height parameter - indicates that there is no step between the current terrain and the previous one. (b) Slope estimate $\hat{\varphi}$. (c) Joint torque $\boldsymbol{\tau}$. (d) Phase diagram of the stance leg (left) and the swing leg (right).

B. Case study on a mixed uneven terrain

To further demonstrate the robustness of our method on uneven terrain, we conducted simulations on a mixed ground consisting of varying slopes and steps. The initial state of the robot was set as $\boldsymbol{X} = [0, 0, 0, 0]^T$, with both legs stationary on the ground. The gentle slope φ_r of the reference limit cycle for each step is set as 2°. The controller parameters were selected as $\boldsymbol{K}_1 = diag(5, 5)$, $\boldsymbol{K}_2 = diag(12, 12)$, $\gamma_1 = 0.3$, $\gamma_2 = 0.3$. In this case study, the re-planning operation was employed. A Bézier curve of degree 5 was constructed to serve as a transition trajectory between the off-track state and the state at $\zeta = 0.8$ on the reference gait.

Fig. 4 illustrates the simulation results. Fig. 4(a) displays a sequential representation of the time lapse animation of the robot walking. It shows the biped robot performs stable virtual passive dynamic walking on the unknown uneven terrain, which illustrates the adaptive controller is efficient in accommodating the significant changes in the slope angle

TABLE III
CONTROLLER PERFORMANCE OF DIFFERENT ζ ON MIXED TERRAIN

ζ	Not Adopted	0.1	0.2	0.3	0.4	0.5	0.6	0.7	0.8	0.9	1
Max torque(Nm)	98.29	1141.8	330.4	171.2	112.4	84.19	68.48	58.73	52.13	47.43	46.42
c_{mt}	0.1362	1.1312	0.3343	0.2058	0.1691	0.1554	0.1486	0.1448	0.1438	0.1459	0.1742

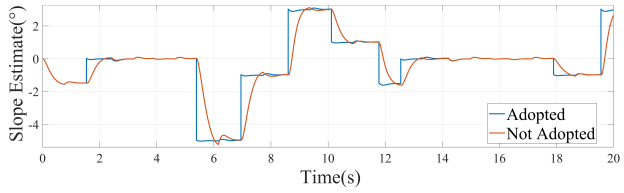

Fig. 5. Simulation results with and without estimation update.

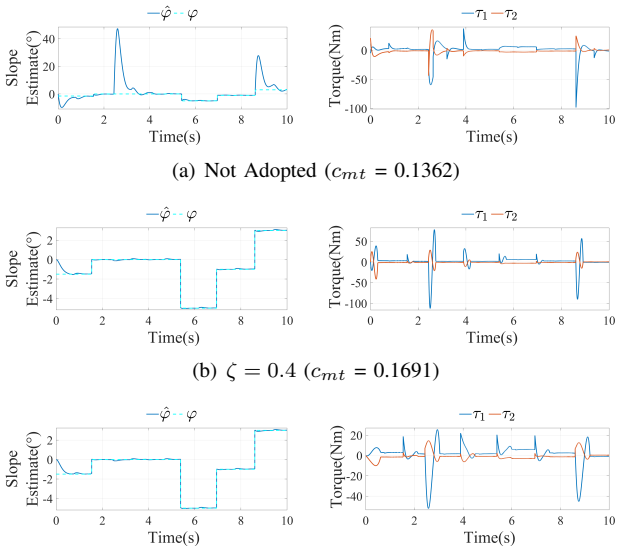

(a) Not Adopted (c_{mt} = 0.1362)

(b) $\zeta = 0.4$ (c_{mt} = 0.1691)

(c) $\zeta = 0.8$ (c_{mt} = 0.1438)

Fig. 6. Simulation results of virtual passive dynamic walking on a mixed terrain of various ζ.

and the step height. Fig. 4(b) shows the slope estimate converges to the true value at the beginning of the motion, and appears to be accurate and smooth subsequently. As shown in Fig. 4(c), the joint torque undergoes significant fluctuations after the terrain changes. This phenomenon is caused by the robot's state lying on the transition trajectory that deviates from passive dynamics. In contrast, the joint torque appears to be straight lines when the robot's state lies on the limit cycle of the reference passive dynamic walking, which is consistent with the characteristics of virtual passive dynamic walking. Fig. 4(d) depicts the phase diagrams of the swing leg and the stance leg, illustrating the robot's trajectory tracking of the reference and re-planned transition trajectories under the proposed controller.

C. Discussion on the slope estimator

Fig. 5 illustrates the impact of estimation update on slope estimation. Comparing simulations with and without estimation update, we observe that utilizing estimation update can lead to faster convergence, whereas the simulation without estimation update still shows slower convergence to true values due to the adaptive law. It is worth mentioning that the estimation update helps bring the slope estimate close to the true value, while the accurate slope estimate merely relies on the adaptive law (17).

D. Discussion on the re-planning

We conducted simulations with various $\zeta \in (0, 1]$ to evaluate the effectiveness of the re-planning strategy against the simulation without it. The maximum joint torque and the c_{mt} corresponding to each ζ are listed in Table. III. As an example, we present the detailed slope estimate and joint torque curves for $\zeta = 0.4$ and $\zeta = 0.8$, along with non-re-planning result in Fig. 6.

Fig. 6 underscores the significance of the re-planning strategy. In simulation without re-planning, slope estimate fluctuations are attributed to the large $\boldsymbol{z}_2$ resulting from the state off-track. However, the introduction of a transition trajectory through re-planning effectively reduces $\boldsymbol{z}_2$ to zero, leading to smoother and more accurate slope estimation.

As illustrated in Table. III, it is noteworthy that the joint torque required to track the re-planned transition trajectory varies significantly depending on different values of ζ. Moreover, ζ ranging from 0.6 to 0.9 yields relatively remarkable c_{mt}, while the c_{mt} of that without re-planning strategy is the lowest. Therefore, it implies that the re-planning strategy results in less effectiveness in terms of energy utilization.

Regarding the maximum joint torque, our qualitative analysis reveals its sensitivity to the ζ parameter when employing the re-planning strategy. In general, a shorter time interval (smaller ζ) required for returning to the reference limit cycle necessitates a higher joint torque. Moreover, theoretically, in the simulation without re-planning, it is influenced by the controller parameters and tracking errors .

VI. CONCLUSION AND FUTURE WORK

This paper proposed an adaptive controller to realize stable virtual passive dynamic walking on unknown uneven terrain. The controller consists of a trajectory tracking law designed using the backstepping method and a slope estimator improved by an estimate update strategy. The simulations show the controller can accurately track the reference passive gait and re-planned transition trajectory, estimate the inclination angle of the terrain, and overcome the impact of terrain changes. Hence the controller is adaptable to the unknown uneven terrain. Our future work will focus on the application of the controller to a 3D robot model with knee joints, and verification on prototypes.

REFERENCES

[1] T. McGeer *et al.*, "Passive dynamic walking," *Int. J. Robotics Res.*, vol. 9, no. 2, pp. 62–82, 1990.

[2] A. Goswami, B. Espiau, and A. Keramane, "Limit cycles and their stability in a passive bipedal gait," in *Proceedings of IEEE international conference on robotics and automation*, vol. 1. IEEE, 1996, pp. 246–251.

[3] J. Zhao, X. Wu, X. Zang, Y. Zhu, and L. Zhu, "The analysis on period doubling gait and chaotic gait of the compass-gait biped model," in *2011 IEEE International Conference on Robotics and Automation*. IEEE, 2011, pp. 2015–2020.

[4] H. Gritli, N. Khraief, and S. Belghith, "Period-three route to chaos induced by a cyclic-fold bifurcation in passive dynamic walking of a compass-gait biped robot," *Communications in Nonlinear Science and Numerical Simulation*, vol. 17, no. 11, pp. 4356–4372, 2012.

[5] S. Collins, A. Ruina, R. Tedrake, and M. Wisse, "Efficient bipedal robots based on passive-dynamic walkers," *Science*, vol. 307, no. 5712, pp. 1082–1085, 2005.

[6] S. H. Collins and A. Ruina, "A bipedal walking robot with efficient and human-like gait," in *Proceedings of the 2005 IEEE international conference on robotics and automation*. IEEE, 2005, pp. 1983–1988.

[7] R. Tedrake, T. W. Zhang, and H. S. Seung, "Stochastic policy gradient reinforcement learning on a simple 3d biped," in *2004 IEEE/RSJ International Conference on Intelligent Robots and Systems (IROS)(IEEE Cat. No. 04CH37566)*, vol. 3. IEEE, 2004, pp. 2849–2854.

[8] A. Smyrli and E. Papadopoulos, "A methodology for the incorporation of arbitrarily-shaped feet in passive bipedal walking dynamics," in *2020 IEEE International Conference on Robotics and Automation (ICRA)*. IEEE, 2020, pp. 8719–8725.

[9] F. Asano, T. Saka, and Y. Harata, "3-dof passive dynamic walking of compass-like biped robot with semicircular feet generated on slippery downhill," in *2016 IEEE International Conference on Robotics and Automation (ICRA)*. IEEE, 2016, pp. 3570–3575.

[10] W. Jia, J. Yang, L. Bi, Q. Zhang, Y. Sun, H. Pu, and S. Ma, "Modelling and analysis of the passive planar rimless wheel mechanism in universal domain," in *2017 IEEE/RSJ International Conference on Intelligent Robots and Systems (IROS)*. IEEE, 2017, pp. 4969–4975.

[11] Y. Zheng, L. Li, F. Asano, C. Yan, X. Zhao, and H. Chen, "Modeling and analysis of tensegrity robot for passive dynamic walking," in *2021 IEEE/RSJ International Conference on Intelligent Robots and Systems (IROS)*. IEEE, 2021, pp. 2479–2484.

[12] W. Znegui, H. Gritli, and S. Belghith, "Design of an explicit expression of the poincaré map for the passive dynamic walking of the compass-gait biped model," *Chaos, Solitons & Fractals*, vol. 130, p. 109436, 2020.

[13] Y. Iwatani and T. Kinugasa, "A necessary condition for passive dynamic walking," in *2022 American Control Conference (ACC)*. IEEE, 2022, pp. 1885–1890.

[14] K. Okamoto, S. Aoi, I. Obayashi, H. Kokubu, K. Senda, and K. Tsuchiya, "Disappearance of chaotic attractor of passive dynamic walking by stretch-bending deformation in basin of attraction," in *2020 IEEE/RSJ International Conference on Intelligent Robots and Systems (IROS)*. IEEE, 2020, pp. 3908–3918.

[15] M. W. Spong and F. Bullo, "Controlled symmetries and passive walking," *IEEE Transactions on Automatic Control*, vol. 50, no. 7, pp. 1025–1031, 2005.

[16] M. W. Spong, J. K. Holm, and D. Lee, "Passivity-based control of bipedal locomotion," *IEEE Robotics & Automation Magazine*, vol. 14, no. 2, pp. 30–40, 2007.

[17] F. Asano, M. Yamakita, N. Kamamichi, and Z.-W. Luo, "A novel gait generation for biped walking robots based on mechanical energy constraint," *IEEE Transactions on Robotics and Automation*, vol. 20, no. 3, pp. 565–573, 2004.

[18] F. Asano, Z.-W. Luo, and M. Yamakita, "Biped gait generation and control based on a unified property of passive dynamic walking," *IEEE Transactions on Robotics*, vol. 21, no. 4, pp. 754–762, 2005.

[19] C. Xu, A. Ming, and M. Shimojo, "A unified framework for virtual passive bipedal gait generation," in *2012 IEEE International Conference on Robotics and Automation*. IEEE, 2012, pp. 3141–3146.

[20] Y. Hu, G. Yan, and Z. Lin, "Feedback control of planar biped robot with regulable step length and walking speed," *IEEE Transactions on Robotics*, vol. 27, no. 1, pp. 162–169, 2010.

[21] I. R. Manchester, U. Mettin, F. Iida, and R. Tedrake, "Stable dynamic walking over uneven terrain," *The International Journal of Robotics Research*, vol. 30, no. 3, pp. 265–279, 2011.

[22] H. Dai and R. Tedrake, "L_2-gain optimization for robust bipedal walking on unknown terrain," in *2013 IEEE international conference on robotics and automation*. IEEE, 2013, pp. 3116–3123.

[23] F. Fan and I. R. Manchester, "Robust control of dynamic walking robots using transverse H_∞," in *2018 IEEE International Conference on Robotics and Automation (ICRA)*. IEEE, 2018, pp. 418–425.

[24] P. Xu, C. Xu, and A. Zheng, "Virtual passive bipedal walking on the irregular ground using kinetic energy tracking control," in *2020 IEEE International Conference on Mechatronics and Automation (ICMA)*. IEEE, 2020, pp. 844–849.

[25] H. K. Khalil, "Nonlinear systems," 1996.

[26] M. S. Branicky, "Multiple lyapunov functions and other analysis tools for switched and hybrid systems," *IEEE Transactions on automatic control*, vol. 43, no. 4, pp. 475–482, 1998.

[27] C. Xu, A. Ming, and Q. Chen, "Characteristic equations and gravity effects on virtual passive bipedal walking," in *2014 IEEE International Conference on Robotics and Biomimetics (ROBIO 2014)*. IEEE, 2014, pp. 1296–1301.